



# The Role of Successive and Interacting CMEs in the Acceleration and Release of Solar Energetic Particles: Multi-viewpoint Observations

Bin Zhuang<sup>1</sup> , Noé Lugaz<sup>1</sup> , Tingyu Gou<sup>2,3</sup> , Liuguan Ding<sup>4</sup> , and Yuming Wang<sup>2,3</sup>

<sup>1</sup>Institute for the Study of Earth, Ocean, and Space, University of New Hampshire, Durham, NH, USA; [bin.zhuang@unh.edu](mailto:bin.zhuang@unh.edu), [noe.lugaz@unh.edu](mailto:noe.lugaz@unh.edu)

<sup>2</sup>CAS Key Laboratory of Geospace Environment, Department of Geophysics and Planetary Sciences, University of Science and Technology of China, Hefei 230026, People's Republic of China

<sup>3</sup>CAS Center for Excellence in Comparative Planetology, University of Science and Technology of China, Hefei 230026, People's Republic of China

<sup>4</sup>School of Physics and Optoelectronic Engineering, Nanjing University of Information Science and Technology, Nanjing 210044, People's Republic of China

Received 2020 May 7; revised 2020 July 21; accepted 2020 August 11; published 2020 September 21

## Abstract

Gradual and large solar energetic particle (SEP) events (flux of ions with energy  $>10$  MeV above 10 pfu) are primarily produced in shocks driven by fast and wide coronal mass ejections (CMEs). Past research, both in theory and statistics, has found that the situation where a fast primary CME (priCME) is preceded by previous CMEs (preCMEs) is favorable to a more efficient particle acceleration. However, the physical causes of this association is still a matter of debate, including the association of the acceleration and release of SEPs with the interaction of successive CMEs. Taking advantage of the twin Solar TERrestrial Relations Observatory spacecraft, we study 41 large SEP events in solar cycle 24 by multi-viewpoint observations. Although 21 events ( $\sim 51\%$ ) have a preCME identifiable in the Large Angle and Spectrometric Coronagraph, we determine that the priCMEs overlap the preCMEs in three dimension (3D) for only 11 events ( $\sim 27\%$ ). We further investigate the acceleration (using type II radio bursts) and release (using velocity dispersion analysis) of the particles for all potential instances of CME–CME interaction in 3D. We find that, for six of 11 events, the priCME is far away from catching up with the preCME when the particles are released. However, for the limited samples, the SEP peak intensity is significantly higher in the events in which the priCME is closest to impacting the preCME, indicating the potential for the increased seed population or more enhanced turbulence levels occurring closer to the preCME.

*Unified Astronomy Thesaurus concepts:* [Solar energetic particles \(1491\)](#); [Solar coronal mass ejections \(310\)](#)

## 1. Introduction

Solar energetic particles (SEPs) are high-energy particles coming from the Sun, which are traditionally categorized as “impulsive” and “gradual” events (Reames 1995, 1999). Historical studies have shown that large gradual SEP events are always associated with interplanetary shocks driven by fast and wide coronal mass ejections (CMEs; e.g., Kahler & Reames 2003; Gopalswamy et al. 2008; Reames 2013), and the correlations between CME properties (e.g., speed, width, or kinetic energy) and SEP peak intensity ( $I_p$ ) have been statistically analyzed (e.g., Gopalswamy et al. 2004; Kahler & Vourlidas 2005, 2013; Richardson et al. 2015; Papaioannou et al. 2016; Kouloumvakos et al. 2019). However, it is found that the relation between the SEP  $I_p$  and CME properties shows a high degree of scatter (e.g., Kahler et al. 2000; Gopalswamy et al. 2004; Cane et al. 2010; Miteva et al. 2013), indicating the importance of other factors in the SEP acceleration process, e.g., the shock seed population, the level of turbulence, the Sun–Earth connectivity, etc. (Wanner & Wibberenz 1993; Kahler 2001; Cliver 2006; Dayeh et al. 2009; Mewaldt et al. 2012; Kozarev et al. 2013, 2019; Richardson et al. 2014; Laitinen et al. 2018; Kahler & Ling 2019; Strauss & le Roux 2019; Xie et al. 2019).

The scenario of a fast primary CME (priCME) associated with one or more preceding CME(s) (preCME) was found to be a possibility to account for an enhanced SEP  $I_p$ . This was first illustrated by Gopalswamy et al. (2002). Later, Gopalswamy et al. (2003, 2004) introduced the term *preconditioning* to describe the effect of a preCME on SEP production, and found a strong correlation between high-particle-intensity events and the existence of preceding CMEs within 24 hr ahead of the

priCMEs. It was then extended to the comparison of SEP events with and without preCMEs to all of solar cycle (SC) 23, showing that the median SEP  $I_p$  was 317 pfu versus 35 pfu ( $1 \text{ pfu} = 1 \text{ proton cm}^{-2} \text{ s}^{-1} \text{ ster}^{-1}$ ) for these two categories (Gopalswamy 2012).

A role for interacting CMEs in SEP production was invoked by Li & Zank (2005), proposing that the shock driven by a preCME can leave a turbulent downstream wake where the enhanced SEP production will occur at the primary CME shock. Later, this work was refined as the “twin-CME” scenario by Li et al. (2012). In this scenario, the preCME and priCME erupt from the same or nearby source regions in a short period; the preCME creates an environment for more efficient particle acceleration with both an excess of seed population and an enhanced turbulence level at the front of the shock driven by the priCME. Based on the “twin-CME” scenario, further studies have looked at specific events, e.g., the 2013 May 22 SEP event (Ding et al. 2014b), or statistics (Ding et al. 2013, 2014a, 2015, 2019). These further supported the enhancement of SEP  $I_p$  within the “twin-CME” eruptions. However, there still exists some ambiguous points from previous studies. Here we investigate three of the main ones, which are described below.

First, do successive CMEs in the “twin-CME” events have spatial overlap in the three-dimensional (3D) space instead of the projected plane? With only single-viewpoint observations, this issue can be solved by limiting the CMEs from the same active region (AR) (Gopalswamy et al. 2004). However, it is unclear whether the two CMEs, especially from the neighboring regions, e.g., in the scenario of sympathetic eruption (Török et al. 2011), can interact with each other meaningfully and low

enough to accelerate protons in the Earth’s direction. The launch of the twin spacecraft of the Solar TERrestrial RELations Observatory (STEREO; Kaiser et al. 2008) enabled the observations of CMEs from multiple viewpoints, and thus the interaction in 3D between CMEs in the corona can be well analyzed (see, e.g., Lugaz et al. 2012; Shen et al. 2013a; Liu et al. 2014; Yashiro et al. 2014; Colaninno & Vourlidas 2015).

Second, does the interaction of successive CMEs play a role in large SEP events? This question was raised by Kahler & Vourlidas (2014). They found that neither the timings of the preCMEs relative to the priCMEs nor the widths, speeds, or numbers of the preCMEs correlate with the SEP Ip. The Ip, as well as the fraction of CMEs with preCMEs, correlates with the 2 MeV proton background intensities. These strongly imply that the higher SEP Ip for priCMEs with preCMEs may not be due primarily to CME–CME interactions, but could be explained by a general increase of both background seed particles and more frequent CMEs during times of higher solar activity. However, they mentioned that the relevance of CME–CME interaction for larger SEP event intensities still remains unclear.

Third, what is the association of the acceleration and release of SEPs with CME–CME interaction, e.g., whether or not the meaningful interaction is necessary for the efficient acceleration and the following release of the particles in the “twin-CME” events? Ding et al. (2014b) found that particle release occurs when the priCME catches up with the trailing edge of the preCME. The time at which particles are first released into the interplanetary space is an important clue to the site and nature of the SEP acceleration mechanism (see Tylka et al. 2003, and references therein). The differences between the CME speeds and the separation of the eruption time ( $\tau$ ) can lead to different interacting types, including the following: (1) no interaction, (2) the shock wave associated with the priCME interacts with the preceding magnetic ejecta (e.g., Lugaz et al. 2005; Scolini et al. 2020), (3) the interaction between two ejecta (see Lugaz et al. 2017, and references therein), and (4) the two-CME-driven shock waves interact. Note that the fourth type could be with or without ejecta–ejecta interacting. In Li et al. (2012), the authors extrapolated that the criterion of  $\tau$  in the “twin-CME” scenario should be  $\sim 9$  hr based on the decay time of the downstream turbulence. Extending it, Ding et al. (2014a) statistically identified that  $\tau \sim 13$  hr based on the large SEP events in SC23. In addition to the “twin-CME” scenario, there are different models to explain the enhancement of SEP intensities driven by consecutive CMEs in different interacting types. For example, Wang et al. (2019) proposed a twin-shock scenario, in which the seed energetic particles produced by the normal preceding shock can be reaccelerated efficiently by the posterior shock catching up with the preceding one. This scenario belongs to the fourth interacting type. Note that in this scenario, the CMEs can erupt from different source regions. Besides, Shen et al. (2008) proposed that a shock–CME interacting complex structure can lead to an extraordinary SEP enhancement only over the entire period of that structure passing through the spacecraft. Recently, Xu et al. (2019) statistically found that the protons’ (with energies from  $\sim 200$  keV to  $\sim 7$  MeV) intensities at 1 au increase more in the events where an interplanetary shock is propagating through a CME structure (e.g., see Lugaz et al. 2015) than for those events which at 1 au are associated with the structures of multiple magnetic clouds. This is especially true in the high-

energy channels, which further supports the result of Shen et al. (2008).

Associated with the SEP events, type II radio bursts are another important aspect that has often been used as a diagnostic for a CME-driven shock (e.g., Kahler 1982; Gopalswamy et al. 2005; Mäkelä et al. 2015; Kahler et al. 2019). Type II radio bursts at metric (M) wavelengths indicate that the shock is generated close to the Sun (e.g.,  $\leq 3 R_s$ ) (Gopalswamy et al. 2009a; Mäkelä et al. 2015), and at decahctometric (DH) wavelengths refer to the existence of the shock in the outer corona or interplanetary space. A radio enhancement following the type II bursts could be used as an indicator of the CME–CME interaction as the transit of the shock front of the fast CME passes through the core of the slow CME (e.g., Gopalswamy et al. 2001b; Démoulin et al. 2007; Ding et al. 2014b; Mäkelä et al. 2016; Lugaz et al. 2017). For example, Gopalswamy et al. (2001b) and Ding et al. (2014b) linked the timing of the enhancement to the interaction, while Mäkelä et al. (2016) used the direction-finding analysis to confirm that the CME–CME interaction region is the source of the type II enhancement. Some other studies have argued that the source of the type II radio enhancement could be the region of the shock-streamer interaction (Shen et al. 2013b; Temmer et al. 2014).

In this paper, we start by focusing on the first question (whether interaction of the successive CMEs even occurs when considering the 3D information), and then investigate the acceleration and release of the SEPs during CME–CME interaction. The second and third points are incorporated in the related analyses. We study the association of the large SEP events with priCMEs and potential preCMEs in SC24, by combining the observations of the instruments at L1 point and STEREO spacecraft. We classify the SEP events into two groups, which are with and without preCMEs, called  $P_{3D}$  and  $NP_{3D}$  (following the terminology in Kahler & Vourlidas 2014, but adding the subscript of 3D to emphasize that the classification is based on multi-viewpoint observations), respectively. We analyze the relationship between the shock formation and solar particle release (SPR) and different types of CME–CME interaction in  $P_{3D}$  group. Our paper is organized as follows: in Section 2, we introduce the observations, the event selection procedure, and the related results; in Section 3, we present the corresponding analyses in  $P_{3D}$  group; and Sections 4 and 5 contain the discussions and conclusions, respectively.

## 2. Large SEP Events in Solar Cycle 24

### 2.1. Observations and Event Selection

We use the list of large SEP events in SC24 from the Coordinated Data Analysis Workshop (CDAW) Data Center<sup>5</sup> (Gopalswamy et al. 2009b). A large SEP event is defined as one with proton intensity  $>10$  pfu in the  $>10$  MeV energy channel of the Geostationary Operational Environmental Satellites (GOES) instrument. In the following analyses, in addition to GOES, we also use the proton data from the Energetic and Relativistic Nuclei and Electron instrument (ERNE; Torsti et al. 1995) on board the Solar and Heliospheric Observatory (SOHO; Domingo et al. 1995) because it contains more energy channels.

<sup>5</sup> [https://cdaw.gsfc.nasa.gov/CME\\_list/sepe/](https://cdaw.gsfc.nasa.gov/CME_list/sepe/)

To identify whether or not a priCME is accompanied by the preCME(s) in 3D, we use the multi-viewpoint observations from the Large Angle and Spectrometric Coronagraph (LASCO; Brueckner et al. 1995) on board SOHO and STEREO/COR, and the CME 3D reconstruction by the graduated cylindrical shell (GCS) model (Thernisien et al. 2006, 2009; Thernisien 2011). Within the GCS model, we assume a CME with a flux-rope structure and with self-similar expansion. The model contains six free parameters to determine the CME shape and position, which are the longitude  $\phi$ , latitude  $\theta$ , height of the leading edge (LE)  $h$ , aspect ratio  $\kappa$ , tilt angle  $\gamma$  with respect to the equator, and half angular width  $\delta$  between the two flux rope legs. The CME 3D speed is derived by a linear fit to the  $h$  at different times, and the CME extent can be described by the face-on angular width ( $w_f$ ) and the edge-on angular width ( $w_e$ ), where  $w_f = 2\delta + w_e$  and  $w_e = 2\sin^{-1}(\kappa)$ . We set the criteria for the identification of a preCME as follows. First, we follow Li et al. (2012) that the waiting time of  $\tau$  between two consecutive CMEs should be less than 9 hr, and  $\tau$  in this paper is estimated by the difference between the first appearance time (FAT<sub>c2</sub>) in LASCO/C2 field of view (FOV) of the two CMEs. Second, the 3D GCS speed and  $w_f$  of the preCME should be larger than  $300\text{ km s}^{-1}$  and  $20^\circ$ , respectively. Third, the priCME should overlap spatially with the preCME in 3D, which can be determined by the GCS results. Note that the value of  $300\text{ km s}^{-1}$  refers to an estimated Alfvén wave speed in the low corona (see Li et al. 2012, and references therein), and  $w_f \geq 20^\circ$  is aimed at excluding narrow CMEs (see Kahler & Vourlidas 2014, and references therein). We note that different criteria will have influence on the identification, and we come back to this point in the discussion section.

## 2.2. Large SEP Events with “Twin” CMEs

Figure 1 shows how the observations from multiple viewpoints can help with the identification of the interaction of CMEs. The SEP event on 2012 July 12 is driven by the priCME with FAT<sub>c2</sub>  $\sim$  16:48 UT. This CME follows a preCME with FAT<sub>c2</sub>  $\sim$  16:24 UT. According to the LASCO observations only (middle panels of Figure 1), it appears that the two CMEs have spatial overlap. However, after combining the observations of the coronagraphs (COR1 and COR2) from STEREO “Ahead” and “Behind” (abbreviated as STA and STB hereafter), it is clear that these two CMEs do not interact with each other. COR1 observations from STA and STB (top left and right panels of Figure 1) clearly show that the preCME is in fact back-sided for the Earth and that the two CMEs propagate  $\sim 90^\circ$  from each other. Reconstruction with the GCS model confirms this finding. This provides a way to uncover the ambiguity of the interaction between successive CMEs in the low corona, especially for those from neighboring source regions.

We focus on 41 large SEP events from the CDAW/SEP list, in which the events from 2014 November to 2015 October are not considered because there were no STEREO data at that period. Table 1 lists the related SEP onset time, Ip, FAT<sub>c2</sub> of the priCME, the location and start time of the solar flare, and the M or DH wavelength range, and the onset time of the type II radio bursts. One can refer to the CDAW/SEP catalog for the detailed information and observations.

In the rest of the article, we use the terms 3D and 2D to refer to the multi-viewpoint and single-viewpoint observations,

respectively. Based on the 3D observations, we identified 11 events in P<sub>3D</sub> group and 30 in NP<sub>3D</sub> group, which are shown in the penultimate column in Table 1. Here we would like to mention two specific events. One is on 2012 March 7 with Ip reaching 6530 pfu, which is associated with two strong halo-CMEs erupting in a very short period. Although it is found that the onset of the particle enhancement is associated with the first eruption (Richardson et al. 2014; Ding et al. 2016; Kouloumvakos et al. 2016), the particle acceleration may be involved with shock–shock interaction within the closely spaced CMEs. Therefore, this event is identified in P<sub>(2)3D</sub> group. The other is on 2017 September 10, with SEP Ip reaching 1490 pfu and driven by an extremely fast CME with speed  $>3000\text{ km s}^{-1}$ . This CME catches up with a merged structure (by two CMEs with FAT<sub>c2</sub> at 16:24 UT and 23:12 UT on September 9, respectively) at  $\sim 68 R_s$  at  $\sim 21:00$  UT (Guo et al. 2018), and it was found that more particles are injected at the catching-up shock through the interaction, which is indicated by a small jump of the GOES data at  $\sim 21:20$  UT (see their Figure 3(d)). However, the GOES observations also show that the proton fluxes are enhanced to a high level in a short time after the priCME eruption, and at this time the priCME is still far away from the preCMEs. Thus, this event is identified in NP<sub>(2)3D</sub> group.

Furthermore, to compare the identification via 3D and 2D observations, we performed again the full identification for the whole set of events. The criteria used here are as follows: (1)  $\tau < 9$  hr, (2) the projected speed and angular width of the preCME should be larger than  $300\text{ km s}^{-1}$  and  $20^\circ$ , and (3) the central position angle of the preCME should lie in the angular expand of the priCME in the projected plane. The CME projected information by LASCO observations can be obtained from the CDAW/CME catalog<sup>6</sup> (Yashiro et al. 2004). The criteria are similar to those used in Ding et al. (2013) and Kahler & Vourlidas (2014), but the values of  $\tau$  and width are slightly different. We identified 21 and 20 events in P<sub>2D</sub> and NP<sub>2D</sub> groups (see the last column in Table 1, and the subscript of 2D indicates the identification by only single-viewpoint observations), respectively. Therefore, after considering the “3D” information, the percentage of the SEP events for priCMEs with preCMEs decreases significantly from 51% (21/41) to 27% (11/41). The percentage of 51% of P<sub>2D</sub> group is slightly lower than but close to the previous value of 65% in Kahler & Vourlidas (2014), but much lower than that of 73% in Ding et al. (2013) which may be because they did not consider a limitation of the angular width of the preCMEs. We note that a similar percentage of 65% was also obtained by Gopalswamy et al. (2004) based on different criteria: (1)  $\tau < 24$  hr, (2) the angular width of a preCME is larger than  $60^\circ$ , and (3) CMEs are from the same source region. These past results are for the SEP-rich events in SC23.

Figure 2 shows the SEP Ip versus the 3D speed of the priCME with SEP events in different groups. The data points with crosses inside refer to the events for which the identifications are opposite by 3D and 2D observations. There are 14 events with the identification changed. The average and median values of the SEP Ip in different groups are given in the figure, showing that the average value in P<sub>(2)3D</sub> group is significantly higher than that in NP<sub>(2)3D</sub> group, but there is no difference between the median values. Furthermore, the

<sup>6</sup> [https://cdaw.gsfc.nasa.gov/CME\\_list/index.html](https://cdaw.gsfc.nasa.gov/CME_list/index.html)

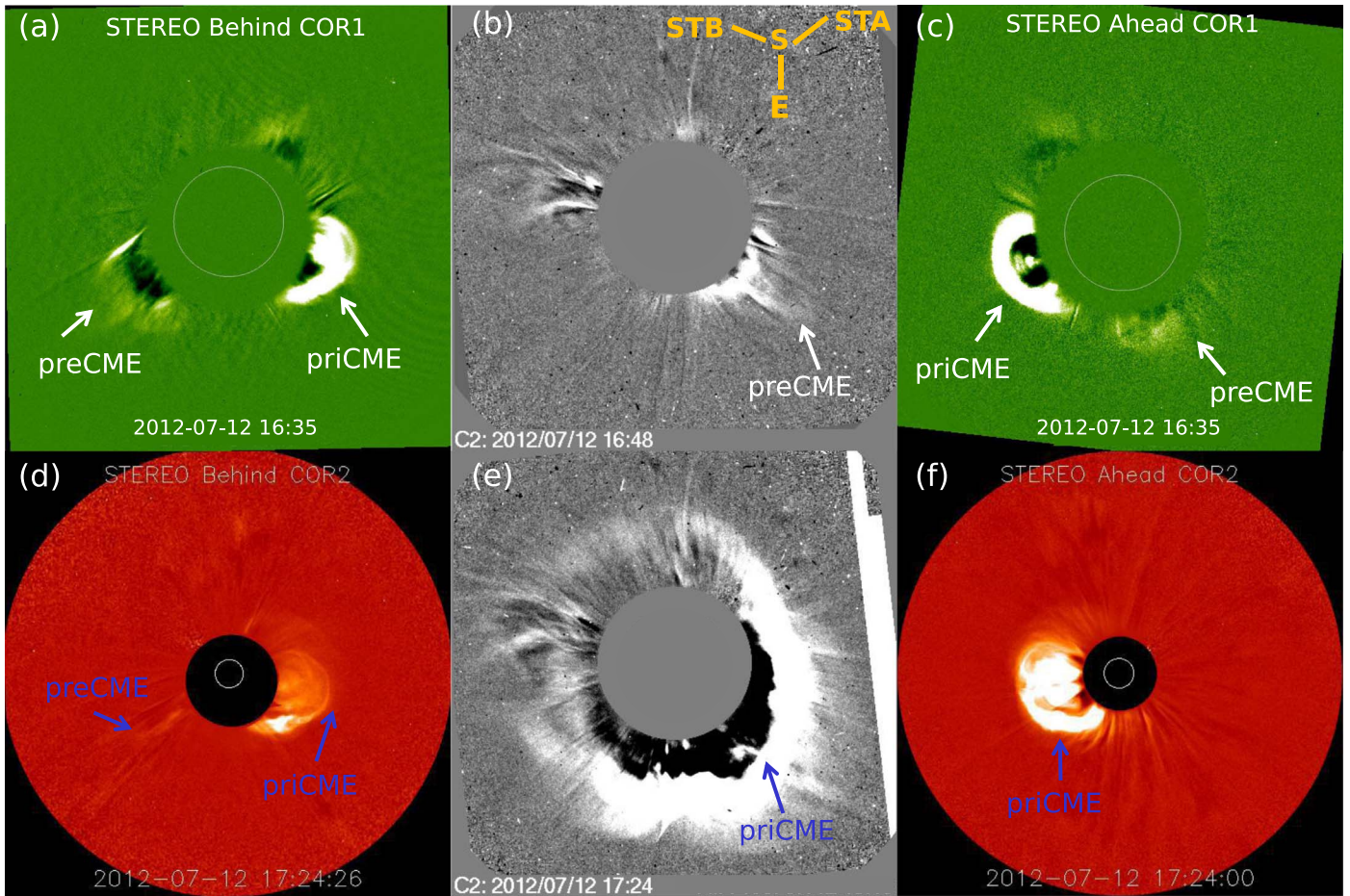


**Figure 1.** Running difference images of the 2012 July 12 series of CMEs as observed by STB/COR1-2 (left), LASCO/C2 (middle), and STA/COR1-2 (right) at two different times. The inset in the top middle panel shows the positions of STA and STB relative to the Sun (S) and the Earth (E) on 2012 July 12. The three images on a given line are at approximately the same time ( $\sim 16:40$  for the top, and  $17:24$  for the bottom).

student’s  $t$ -test (TM\_TEST.PRO in Interactive Data Language software) is then applied to the two groups in 3D and 2D, respectively, and the results show that the 3D but not the 2D groups are statistically different in terms of their  $I_p$ . Figure 2 also shows the relationship between CME 3D speed and SEP  $I_p$  with the correlation coefficient (cc) in the bottom right corner: (1) cc value of 0.54 and 0.54 in  $NP_{3D}$  and  $NP_{2D}$ , respectively, and (2) the better correlation of  $cc = 0.62$  in  $P_{2D}$  and  $cc = 0.71$  in  $P_{3D}$ . We note a similar comparison of the cc between  $P_{2D}$  and  $NP_{2D}$  in Gopalswamy et al. (2004) for the successive CMEs from the same AR, giving that the cc in  $NP_{2D}$  is higher than that in  $P_{2D}$  (0.58 versus 0.43). Furthermore, it is found that the slope of the linear fit to the data points in  $P_{(2)3D}$  group is larger than that in  $NP_{(2)3D}$  group, which is consistent with those in Gopalswamy et al. (2004).

### 3. Acceleration and Release of SEPs in “Twin-CME” Events

#### 3.1. Method and Result

##### 3.1.1. SEP Event on 2012 January 23

In this section, we investigate the acceleration and release of SEPs during CME–CME interaction, and we use an SEP event on 2012 January 23 (with onset time at 04:45 UT) to illustrate our analyses. This case with two consecutive CMEs from the same source region, AR 11402, was widely studied in previous

research, such as the related flux ropes in the corona (Li & Zhang 2013), or the analyses by multiwavelength observations (Joshi et al. 2013). Figure 3 shows the proton fluxes in different energy channels measured by GOES, in which the vertical dashed line denotes the SEP onset time. The acceleration of the particles is related to the shock formation in the low corona, which can be marked by the onset of the type II radio bursts. To estimate the SPR time, the velocity dispersion analysis (VDA, and see Tylka et al. 2003; Reames 2009a; Gopalswamy et al. 2012; Vainio et al. 2013) is used here. In VDA, SEPs with different energies are assumed to be released at the same time and the same location near the Sun, and transport along the same path. Plotting the onset times ( $t_{\text{onset}}$ ) at different energy channels versus  $v^{-1}$  ( $v$  is the proton speed) can yield a line with the SPR time as the intercept and the magnetic path length as the slope. Here  $t_{\text{onset}}$  is identified by  $f(t_{\text{onset}}) = \langle f \rangle + 3\sigma$ , where  $\langle f \rangle$  is the average intensity of the pre-event background in a 6 hr period and  $\sigma$  is its standard deviation. One can refer to the detailed procedures in Ding et al. (2014b). The VDA results are shown in the insert in Figure 3, giving the initial release time and path length as 04:14 ( $\pm 00:05$ ) UT and 1.36 ( $\pm 0.12$ ) au, respectively. To compare the release time to the CME and radio observations at 1 au, the light travel time of  $\sim 8.3$  minutes should be added to the SPR times, i.e., 04:22 UT for this case.

**Table 1**  
Large SEP Events in SC24

SEP Event		CME FAT <sub>C2</sub>	Flare		Type II		Group	
Onset Time	Ip		Loc	ST	WR	OT	Obs. <sub>3D</sub>	Obs. <sub>2D</sub>
2010 Aug 14 11:05	14	10:12	N17W52	09:38	M	09:52	NP <sub>3D</sub>	NP <sub>2D</sub>
2011 Mar 7 21:45	50	20:00	N31W53	19:43	M, DH	19:54	NP <sub>3D</sub>	P <sub>2D</sub>
2011 Mar 21 04:10	14	02:24	>W90b	...	...	...	NP <sub>3D</sub>	NP <sub>2D</sub>
2011 Jun 7 07:20	72	06:49	S21W54	06:16	M, DH	06:25	NP <sub>3D</sub>	NP <sub>2D</sub>
2011 Aug 4 04:30	96	04:12	N19W36	03:49	M, DH	03:54	NP <sub>3D</sub>	NP <sub>2D</sub>
2011 Aug 9 08:20	26	08:12	N17W69	07:59	M, DH	08:01	P <sub>3D</sub>	P <sub>2D</sub>
2011 Sep 22 17:55	35	10:48	N09E89	10:29	M, DH	10:39	NP <sub>3D</sub>	P <sub>2D</sub>
2011 Nov 26 08:15	80	07:12	N17W49	06:09	DH	07:15	P <sub>3D</sub>	NP <sub>2D</sub>
2012 Jan 23 04:45	6310	04:00	N28W21	03:38	DH	04:00	P <sub>3D</sub>	P <sub>2D</sub>
2012 Jan 27 18:55	795	18:27	N27W71	18:03	M, DH	18:10	NP <sub>3D</sub>	NP <sub>2D</sub>
2012 Mar 7 02:50	6530	00:24	N17E27	00:13	M, DH	00:17	P <sub>3D</sub>	P <sub>2D</sub>
2012 Mar 13 18:05	469	17:36	N17W66	17:12	M, DH	17:15	NP <sub>3D</sub>	NP <sub>2D</sub>
2012 May 17 01:55	255	01:48	N11W76	01:25	M, DH	01:31	P <sub>3D</sub>	NP <sub>2D</sub>
2012 May 26 23:25	14	20:57	>W90b	...	M	20:47	NP <sub>3D</sub>	NP <sub>2D</sub>
2012 Jun 14 23:25	15	14:12	S17E06	12:52	...	...	NP <sub>3D</sub>	NP <sub>2D</sub>
2012 Jul 7 00:05	25	23:24 <sup>-1</sup>	S13W59	23:01 <sup>-1</sup>	M, DH	23:09 <sup>-1</sup>	NP <sub>3D</sub>	NP <sub>2D</sub>
2012 Jul 8 18:10	19	16:36	S17W74	16:23	M, DH	16:30	P <sub>3D</sub>	P <sub>2D</sub>
2012 Jul 12 17:25	96	16:48	S15W01	16:16	M, DH	16:25	NP <sub>3D</sub>	P <sub>2D</sub>
2012 Jul 17 15:30	136	13:48	S28W65	13:19	DH	14:40	NP <sub>3D</sub>	NP <sub>2D</sub>
2012 Jul 19 06:40	80	05:24	S13W88	04:17	M, DH	05:24	NP <sub>3D</sub>	NP <sub>2D</sub>
2012 Jul 23 08:00	12	02:36	>W90	...	...	...	NP <sub>3D</sub>	NP <sub>2D</sub>
2012 Sep 1 01:25	60	20:00 <sup>-1</sup>	S25E59	19:45 <sup>-1</sup>	M, DH	19:42	NP <sub>3D</sub>	P <sub>2D</sub>
2012 Sep 28 01:20	28	00:12	N06W34	23:36	M, DH	23:44	NP <sub>3D</sub>	NP <sub>2D</sub>
2013 Mar 15 19:40	16	07:12	N11E12	05:46	DH	07:00	NP <sub>3D</sub>	NP <sub>2D</sub>
2013 Apr 11 08:25	114	07:24	N09E12	06:56	M, DH	07:02	NP <sub>3D</sub>	P <sub>2D</sub>
2013 May 15 06:35	42	01:48	N12E64	01:25	M, DH	01:37	P <sub>3D</sub>	P <sub>2D</sub>
2013 May 22 14:20	1660	13:25	N15W70	13:08	M, DH	12:59	P <sub>3D</sub>	P <sub>2D</sub>
2013 Jun 23 08:30	14	03:12 <sup>-2</sup>	S16E73	02:30 <sup>-2</sup>	DH	03:36 <sup>-2</sup>	NP <sub>3D</sub>	NP <sub>2D</sub>
2013 Sep 30 00:25	182	22:12 <sup>-1</sup>	N17W29	20:42 <sup>-1</sup>	DH	21:53 <sup>-1</sup>	NP <sub>3D</sub>	NP <sub>2D</sub>
2013 Dec 28 19:00	29	17:36	>W90	...	DH	17:31	NP <sub>3D</sub>	P <sub>2D</sub>
2014 Jan 6 08:15	42	08:00	>W90	07:30	M, DH	07:45	P <sub>3D</sub>	P <sub>2D</sub>
2014 Jan 7 19:55	1026	18:24	S15W11	18:04	M, DH	18:17	NP <sub>3D</sub>	P <sub>2D</sub>
2014 Feb 20 08:15	22	08:00	S15W73	07:26	M, DH	07:45	NP <sub>3D</sub>	P <sub>2D</sub>
2014 Feb 25 03:50	24	01:25	S12E82	00:39	M, DH	00:56	NP <sub>3D</sub>	P <sub>2D</sub>
2014 Apr 18 13:40	58	13:25	S20W34	12:31	M, DH	12:55	P <sub>3D</sub>	P <sub>2D</sub>
2014 Sep 10 21:35	126	18:00	N14E02	17:21	DH	17:45	NP <sub>3D</sub>	P <sub>2D</sub>
2016 Jan 2 00:15	22	23:24 <sup>-1</sup>	S25W82	23:10 <sup>-1</sup>	M, DH	23:21 <sup>-1</sup>	NP <sub>3D</sub>	NP <sub>2D</sub>
2017 Jul 14 04:40	22	01:25	S06W29	01:07	DH	01:18	NP <sub>3D</sub>	P <sub>2D</sub>
2017 Sep 4 22:30	210	20:12	S10W12	20:28	DH	20:27	P <sub>3D</sub>	P <sub>2D</sub>
2017 Sep 6 12:35	844	12:24	S08W33	11:53	M, DH	12:02	NP <sub>3D</sub>	P <sub>2D</sub>
2017 Sep 10 12:35	1490	16:00	>W90b	15:35	M	15:53	NP <sub>3D</sub>	NP <sub>2D</sub>

#### Notes.

[1] The table lists the information about the SEP onset time, Ip, CME first appearance time in LASCO/C2 FOV (FAT<sub>C2</sub>), the location and start time (ST) of the flare, the wavelength range (M or DH) and the onset time (OT) of the type II radio bursts, and the type of group every event belongs to. [2] The superscript of “-1” or “-2” indicates one (two) day(s) prior to the SEP onset day.

We then use the GCS model to analyze the CME propagation and interaction in 3D. The parameters in the model are described in Section 2.1, and the fitting procedures are: (1) selecting a time when the CME is at a relatively higher height and well observed by LASCO and STEREO simultaneously, (2) adjusting all the parameters to make the constructed flux rope overlap best with the CME observed in the coronagraphs, and (3) changing the time backward and forward and adjusting  $h$  but fixing the left five parameters. The top part of Figure 4 shows the observations of two CMEs in STB/COR2, LASCO/C2, and STA/COR2 at approximately the same time (04:00 UT), respectively, and the bottom part overlaps the flux ropes (red for the preCME and green for the priCME) as modeled by the GCS model. The fitted parameters

for the preCME are  $\phi = 22^\circ.9$ ,  $\theta = 23^\circ.4$ ,  $h = 6.75 R_s$ ,  $\kappa = 0.4$ ,  $\gamma = -79^\circ.2$ , and  $\delta = 28^\circ.8$ ; for the priCME,  $\phi = 15^\circ.7$ ,  $\theta = 41^\circ.4$ ,  $h = 4.45 R_s$ ,  $\kappa = 0.5$ ,  $\gamma = 84^\circ.6$ , and  $\delta = 68^\circ.4$ . Evident from the figure and the fitted parameters, there exists an interaction between the two CMEs.

Figure 5 shows the variation of the heights of the LE and trailing edge (TE,  $h_t = h - 2r = \frac{1-\kappa}{1+\kappa}h$ , where  $r = \frac{\kappa}{1+\kappa}h$  is the cross-section radius along the propagation direction) of the preCME, and the LE of the priCME at different times. The vertical black dotted line denotes the SPR time with two thick bars at top and bottom axes indicating the corresponding uncertainties, and the blue line denotes the onset time of the DH type II radio bursts. The uncertainty of  $h$  is set as  $0.48 R_s$  (Thernisien et al. 2009), and the black, green and red dashed

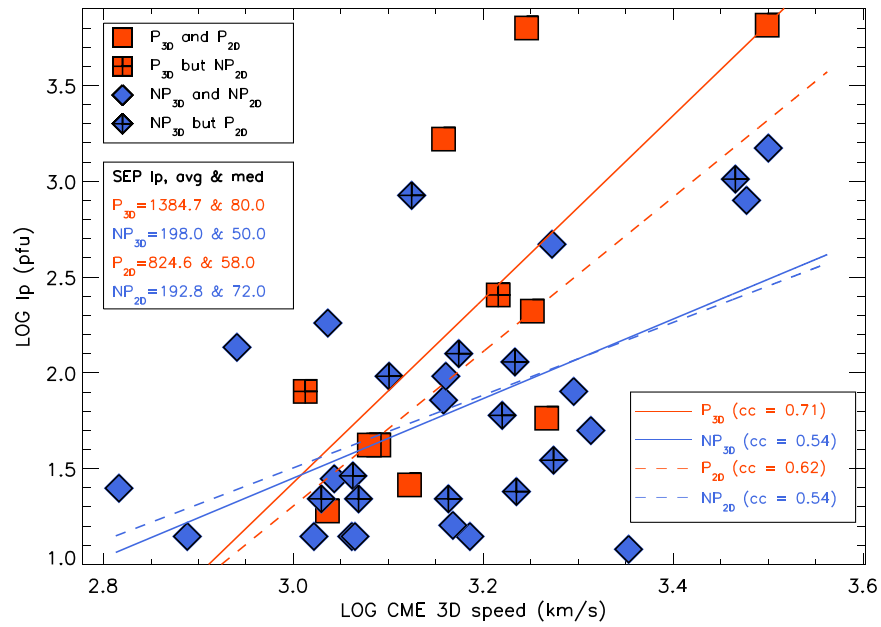


**Figure 2.** Peak intensity ( $I_p$ ) of the SEP vs. 3D speed of the primary CME (priCME) associated with the events. The red square refers to  $P_{3D}$  group and the blue diamond refers to  $NP_{3D}$ . The symbols with crosses inside indicate the identification by 3D and 2D observations are opposite. The solid (dashed) lines indicate the linear fit to the data points in  $P_{3D(2D)}$  (orange) and  $NP_{3D(2D)}$  (blue) groups, respectively. The correlation coefficients (cc) of the CME 3D speed vs. SEP  $I_p$  in different groups are shown in the bottom right corner. The insert in the left part gives the average and median values of the SEP  $I_p$ .

lines show the results of the linear fit to  $h$ . The priCME is found to be much faster than the preCME. In this case, we stop plotting the black and green lines when the LEs of two CMEs are rightly intersected, because in observations the priCME overlaps the preCME entirely after 04:24 UT, making it impossible to distinguish between the two CMEs. Furthermore, the angular separation between the propagation directions of two CMEs should be considered, and thus we project the red line to the direction of the preCME, which is shown by the orange dashed line. We find that the proton release time occurs  $\sim 40$  minutes after the LE of the priCME catches up with the TE of the preCME. This interaction may be related to the third or fourth interacting type as described in Section 1, and the in situ observations at 1 au confirms the interacted structure (Joshi et al. 2013). The DH type II bursts (associated with an enhancement) start at  $\sim 04:00$  UT, which is roughly the time the LE of the priCME reaches the core of the preCME.

In the following cases, we do the similar analyses on the SEP and CME observations. Table 2 gives a summary about the SEP onset time, the SPR time, the  $FAT_{C2}$ , 2D and 3D parameters of the preCME and priCME, the start time of the CME–CME interaction (which refers to the time when the LE of the priCME catches up with the TE of the preCME), and the onset time of the type II bursts. Here we do not go over the case on 2013 May 22 as it was studied by Ding et al. (2014b), but the related information is also listed in Table 2. In this event, the two CMEs are from the neighboring source regions, and the SPR occurs slightly earlier (9 minutes) than but close to the start of the interaction.

### 3.1.2. SEP Event on 2011 August 9

The SEP event on 2011 August 9 with onset time at 08:20 UT is driven by the CME (priCME) with  $FAT_{C2} \sim 08:12$  UT, which was previously studied by Gopalswamy et al. (2013). Based on the 3D observations, the related preCME is identified as the CME with  $FAT_{C2} \sim 03:48$  UT. These two CMEs are

from the same source region, AR 11263. Applying the VDA to the SOHO/ERNE proton data, we derive the SPR time (with the light travel time of  $\sim 8.3$  minutes added) and the path length as 08:05 ( $\pm 00:04$ ) UT and 1.09 ( $\pm 0.11$ ) au, respectively. Figure 6(a) shows the information about the type II radio bursts, SPR and CME–CME interaction. It is found that the priCME starts to impact the preCME at  $\sim 09:20$  UT, which is 75 minutes after the SPR. Furthermore, the SPR time is close to the onset time of the M type II bursts (08:01 UT), indicating that the protons are accelerated and then released shortly when the shock is formed in the low corona.

### 3.1.3. SEP Event on 2011 November 26

The SEP event on 2011 November 26 with onset time at 08:15 UT, which was studied by Gopalswamy et al. (2015) focusing on the related filament eruption, is driven by the CME (priCME) with  $FAT_{C2} \sim 07:12$  UT, and the preCME is identified to start with  $FAT_{C2} \sim 00:36$  UT. Both CMEs are found to be from neighboring source regions. Note that the 2D speed by the linear fit of the preCME is  $292 \text{ km s}^{-1}$ , smaller than  $300 \text{ km s}^{-1}$ ; but the 3D one is  $341 \text{ km s}^{-1}$ . The VDA based on SOHO/ERNE data gives the SPR time (with 8.3 minutes added) and the path length as 07:31 ( $\pm 00:25$ ) UT and 2.36 ( $\pm 0.22$ ) au, respectively. Figure 6(b) shows the information about the type II radio bursts, SPR, and CME–CME interaction, and it is found that the LE of the priCME catches up with the TE of the preCME at  $\sim 08:10$  UT (the intersection of the orange and green lines). The SPR is found to occur prior to the start of the interaction by  $\sim 40$  minutes. Furthermore, the onset of the DH type II bursts is  $\sim 15$  minutes prior to the SPR, and an enhancement occurs around 09:24 UT,  $\sim 74$  minutes after the start of the interaction; no M type II bursts were present in this event, indicating that the shock may be formed beyond  $2\text{--}3 R_s$  (Gopalswamy et al. 2015).

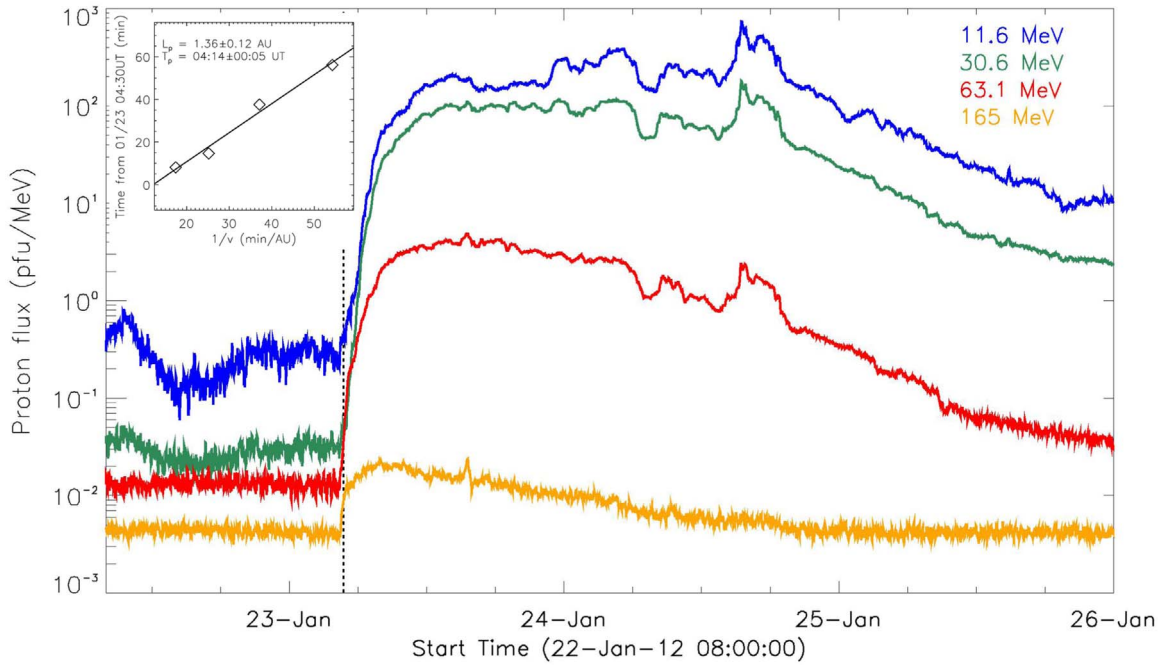


**Figure 3.** The profiles of the proton fluxes at different energy channels detected by GOES for the “twin-CME” event on 2012 January 23. The vertical dashed line indicates the onset of the SEP event, and the insert shows the related VDA results.

### 3.1.4. SEP Event on 2012 March 7

The SEP event on 2012 March 7 with onset time at 02:50 UT is believed to be driven by the CME with  $FAT_{C2} \sim 00:24$  UT (Richardson et al. 2014; Ding et al. 2016; Kouloumvakos et al. 2016). This event with extremely high  $I_p$  of 6530 pfu may be involved with enhancement of the particle acceleration by shock–shock interaction, while there is a fast halo CME closely following the first CME with  $FAT_{C2} \sim 01:30$  UT (Richardson et al. 2014). These two CMEs are from the same source region, AR 11429. The VDA result was given by Ding et al. (2016), showing the SPR time (with 8.3 minutes added) and the path length as 00:38 ( $\pm 00:01$ ) UT and 2.06 ( $\pm 0.04$ ) au, respectively. The onset of the M (DH) type II radio bursts is at  $\sim 00:17$  (01:00) UT. Figure 6(c) shows the information about the radio bursts, SPR, and CME–CME interaction, and it shows that the protons are accelerated and then released before the LE of the second CME catches up with the TE of the first CME.

### 3.1.5. SEP Event on 2012 May 17

The SEP event on 2012 May 17 with onset time at 01:55 UT is driven by the priCME with  $FAT_{C2} \sim 01:48$  UT. However, in the LASCO images, we could only observe one CME (also in CDAW/CME catalog). Shen et al. (2013a) made an identification of the preCME based on the Atmospheric Imaging Assembly (AIA; Lemen et al. 2012) on board the Solar Dynamics Observatory (SDO; Pesnell et al. 2012) and STEREO/COR1. These two CMEs overlap shortly after their eruption from the same source region, AR 11476, making them indistinguishable in LASCO FOV. The VDA based on SOHO/ERNE data gives the SPR time (with 8.3 minutes added) and the path length as 01:39 ( $\pm 00:05$ ) UT and 1.19 ( $\pm 0.14$ ) au, respectively. Figure 6(d) shows the information about the type II radio bursts, SPR, and CME–CME interaction. Because of the completed overlap in LASCO FOV, the black and green dashed lines are stopped after the overlap, and the orange line is

not shown here. Note that even though the two CMEs start interacting very early in the low corona, the SPR occurs when the priCME reaches the height of  $\sim 2 R_s$ , and this is also found by Gopalswamy et al. (2013), given that the CME height at SPR time is  $2.32 R_s$ . At the SPR time the LEs of both CMEs are close to each other. Wang et al. (2019) used a scenario of twin-shock interaction to explain this phenomenon, in which the particles can be efficiently accelerated at the pileup collision of the twin shock. Similarly, Shen et al. (2013a) proposed that this case is slightly different from the “twin-CME” scenario because the two CMEs occur in very close succession; the particles being accelerated as they bounce between the two shocks could act as the major reason for an efficient acceleration. The onset of the type II bursts is  $\sim 8$  minutes before the SPR; Shen et al. (2013a) gave two episodes of the enhanced radio emissions, and the first (01:42–01:48 UT) and second (02:00–02:08 UT) were thought to be caused by the priCME driven shock interacting with the preCME and the interaction of the two shocks, respectively.

### 3.1.6. SEP Event on 2012 July 8

The SEP event on 2012 July 8 with onset time at 18:10 UT is driven by the priCME with  $FAT_{C2} \sim 16:36$  UT, and the preCME is identified with  $FAT_{C2} \sim 10:48$  UT. These two CMEs are from the same source region, AR 11515. The VDA based on GOES data gives the SPR time (with 8.3 minutes added) and the path length as 17:02 ( $\pm 00:27$ ) UT and 3.98 ( $\pm 0.73$ ) au, respectively. Note that the estimated path length is larger than the normal length from 1.1 to 2.2 au (Reames 2009b), and it may be due to the fact that the latitude of propagation of the priCME is S49, which is significantly away from the ecliptic plane. In Figure 6(e), it is found that the proton is initially released  $\sim 100$  minutes before the start of the CME–CME interaction. The onset time of the M type II radio bursts is 16:30 UT, indicating the formation of the CME-driven shock and the corresponding particle acceleration, and it is  $\sim 32$

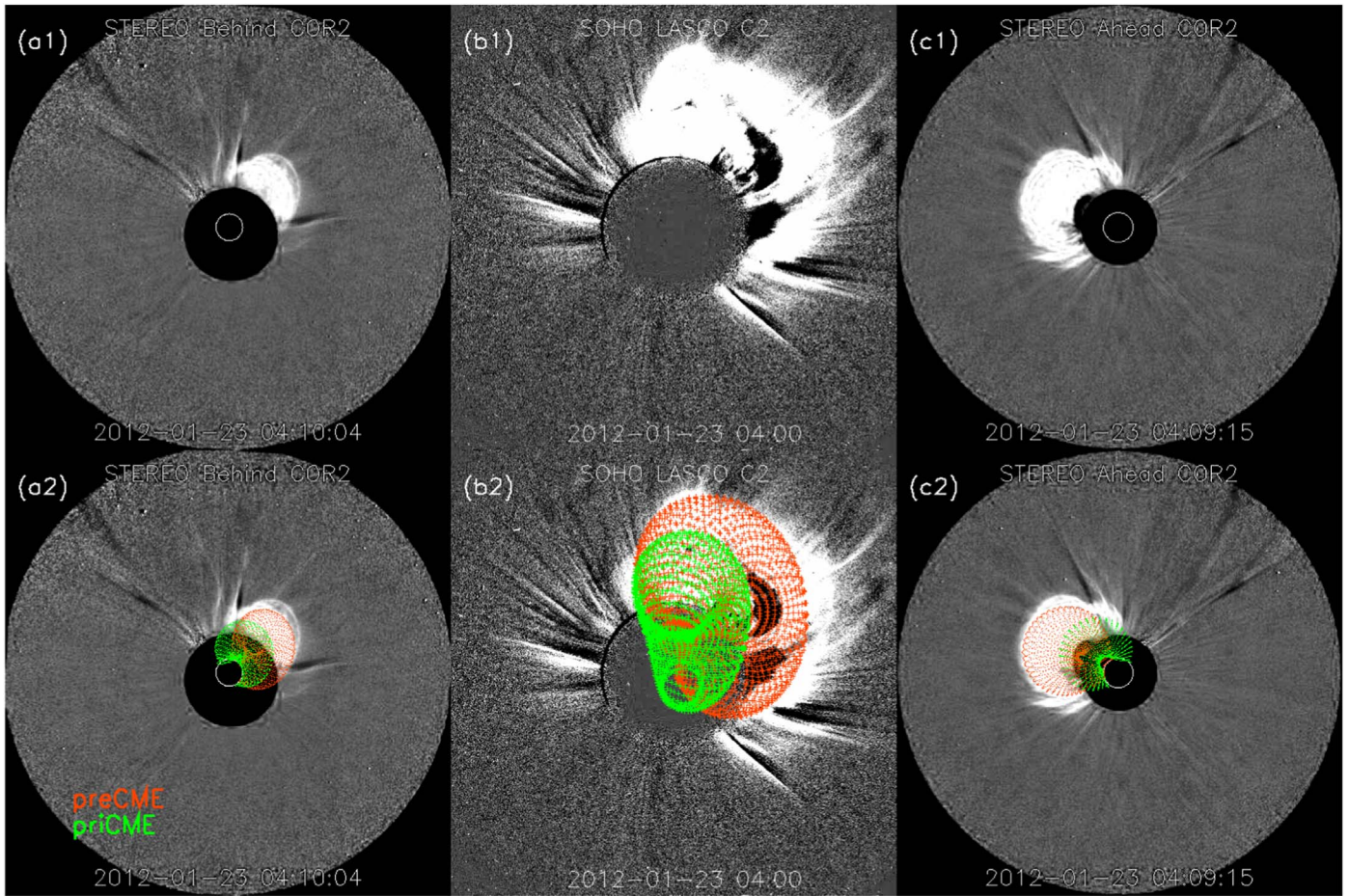


**Figure 4.** Construction of two CMEs on 2012 January 23 using the GCS model. The upper panels show the observations by STB/COR2, LASCO/C2, and STA/COR2 at approximately the same time (04:00 UT). The lower panels show the constructed flux ropes of these two CMEs. In addition, the early evolution of the priCME in the low corona is clearer in COR1/FOV around 03:50 UT.

minutes prior to the SPR time. In addition, a radio enhancement is found to start at  $\sim 19:10$  UT, which may be related to the CME–CME interaction.

### 3.1.7. SEP Event on 2013 May 15

The SEP event on 2013 May 15 with onset time at 06:35 UT is driven by the priCME with  $FAT_{C2} \sim 01:48$  UT, and the preCME is identified with  $FAT_{C2} \sim 22:12$  UT on May 14 from a neighboring source region (though there were six CMEs having similar propagation directions during the interval of 9 hr from the CDAW/CME catalog). Applying the VDA to the SOHO/ERNE proton data, we obtain the SPR time (with 8.3 minutes added) and the path length as 06:34 ( $\pm 00:18$ ) UT on May 15 and 3.25 ( $\pm 0.45$ ) au, respectively. Here the SEP onset is much later than the priCME eruption and the VDA results may not be reliable, due to the eastward priCME having poor magnetic connectivity with the observers near the Earth. Figure 6(f) shows the interaction between the priCME and preCME, and the start of the interaction is found to be at  $\sim 04:00$  UT, which is prior to the SPR by more than 2 hr. Actually, if we follow the assumption that the particle acceleration occurs at  $\sim 4 R_{\odot}$  (Reames 2009b; Gopalswamy et al. 2010; Li et al. 2012), then we can estimate the SPR time (adding the light travel time) to be 01:56 UT (shown by the horizontal and vertical dotted lines), which is  $\sim 21$  minutes after the onset of the M type II radio bursts, indicating the SPR

occurs shortly after the shock forms in the low corona. At this case, the SPR time is  $\sim 125$  minutes prior to the start of the interaction. Note that the SEP Ip of this event is 42 pfu, but we should know that it is influenced by the poor magnetic connectivity (see Section 4.2).

### 3.1.8. SEP Event on 2014 January 6

The SEP event on 2014 January 6 with onset time at 08:15 UT, also studied by Thakur et al. (2014), is driven by the priCME with  $FAT_{C2} \sim 08:00$  UT, and the related preCME is identified as the CME with  $FAT_{C2} \sim 00:36$  UT. These two CMEs are from the same source region, which is determined by the Extreme Ultraviolet Imager (EUVI, Howard et al. 2008) on board STA. Applying the VDA to the GOES proton data, we derive the SPR time (with 8.3 minutes added) and the path length as 07:47 ( $\pm 10$ ) UT and 1.77 ( $\pm 0.29$ ) au, respectively. Figure 6(g) shows the CME–CME interaction associated with the type II radio bursts and the VDA result, in which the time of the start of the CME–CME interaction is found to be  $\sim 09:25$  UT,  $\sim 100$  minutes later than the SPR time. The onset of the M type II bursts (07:45 UT) is consistent with the SPR onset, but there is no observation of an enhancement.

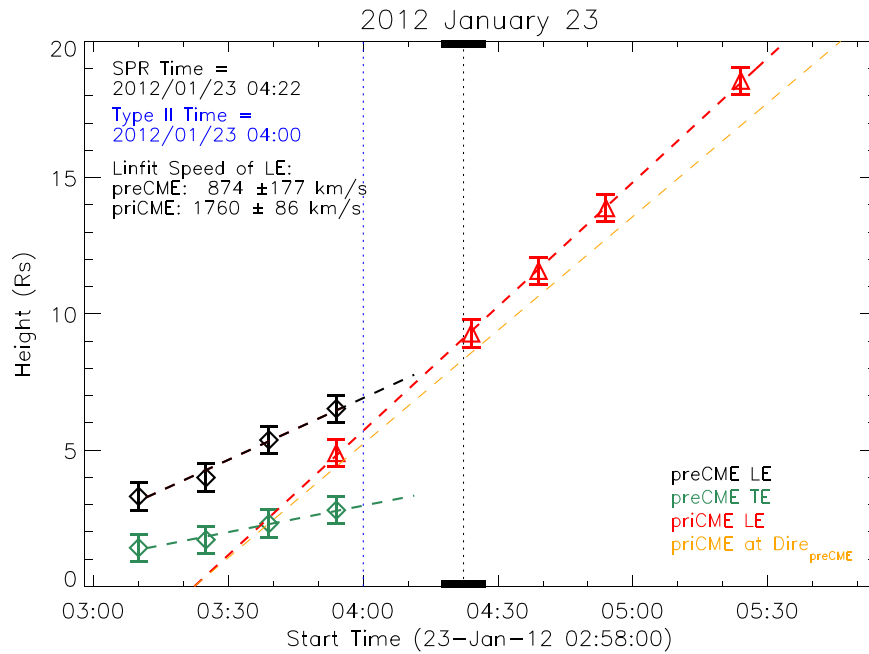


**Figure 5.** SEP event on 2012 January 23: the interaction between the preCME and the priCME. The black, green, and red diamonds depict the GCS model heights of the LE and TE of the preCME, and LE of the priCME, respectively. The dashed lines indicate the linear fit to the data points, and the orange one is the projection of the red line to the direction of the preCME. The vertical black and blue dotted lines mark the corrected SPR time and the onset time of the DH type II radio bursts, respectively, and the two thick bars at the top and bottom axes are related to the uncertainties of the SPR time.

### 3.1.9. SEP Event on 2014 April 18

The SEP event on 2014 April 18 with onset time with 13:40 UT is driven by the priCME with  $FAT_{C2} \sim 13:25$  UT, and the preCME is identified as the CME with  $FAT_{C2} \sim 07:24$  UT). These two CMEs are found to be from the same source region, AR 12036. Applying the VDA to the SOHO/ERNE proton data, we derive the SPR time (with 8.3 minutes added) and the path length as  $13:25 (\pm 6)$  UT and  $1.31 (\pm 0.16)$  au, respectively. Figure 6(h) shows the CME–CME interaction associated with the type II radio bursts and the VDA result, in which the start time of the interaction is found to be  $\sim 13:50$  UT, which is 25 minutes later than the SPR time. The onset of the M type II bursts is at  $\sim 12:55$  UT,  $\sim 30$  minutes prior to the SPR time. Besides, it is found that there exists a radio enhancement in the period of  $\sim 14:30$  to  $15:00$  UT, which might be an indicator of the CME–CME interaction.

### 3.1.10. SEP Event on 2017 September 4

The SEP event on 2017 September 4 with onset time at 22:30 UT is driven by the priCME with  $FAT_{C2} \sim 20:36$  UT. At this time, there were no data from STB. The preCME is identified as the CME with  $FAT_{C2} \sim 19:00$  UT. These two CMEs are found to be from the same source region of AR 12673. The interaction of these two CMEs was previously studied by Shen et al. (2018), focusing on the influence of the interaction on the related geoeffectiveness. In this case, we met two problems in obtaining the SPR time: (1) the data gap of SOHO/ERNE and (2) only two energy channels of GOES properly used for the VDA. Therefore, we take two methods: (1) applying the VDA to the GOES data in the limited energy channels, and (2) calculating the transport time of protons at the energy of 10 MeV with the length of the nominal Parker spiral. Based on the VDA, the SPR time and the path length are 21:38 UT and 1.6 au, respectively, without the calculation of the

uncertainties. The nominal Parker spiral length is found to be 1.10 au with an estimated solar wind speed of  $500 \text{ km s}^{-1}$ , and it results in the transport time of the  $E = 10$  MeV proton to be  $\sim 63$  minutes, indicating that the SPR time should be 21:27 UT, which is close to the VDA result. Figure 6(i) shows the GCS model results of the two CMEs, and the start of the interaction is found to be at 20:45 UT, nearly 1 hr prior to the estimated SPR time. The estimated SPR time leads the SPR height to be  $\sim 12 R_s$ , which may refer to the scenario that the background magnetic field lines are highly disturbed by the strong preCME or the presence of closed lines may delay the particle release. We note that under the assumption that the SPR height is at  $4 R_s$ , the SPR time (adding the light travel time) is estimated to be 20:38 UT (shown by the horizontal and vertical dotted lines), which is  $\sim 9$  minutes after the onset of the DH type II radio bursts. In that case, we can deduce that the SPR is slightly (7 minutes) prior to the start of the CME–CME interaction.

### 3.2. SEP Events Associated with Different Types of CME–CME Interaction

Based on the above analyses (SPR at  $4 R_s$  is used for the events on 2013 May 15 and 2017 September 4), we find that, among the 11 SEP cases, six (events on 2011 August 9, 2011 November 6, 2012 July 8, 2013 May 15, 2014 January 6, and 2014 April 18) have SPR much before the start of the CME–CME interaction, two (events on 2013 May 22 and 2017 September 4) have SPR close to the start of the interaction, two (events on 2012 January 23 and 2012 May 17) have SPR after the start of the interaction, and one (on 2012 March 7) is driven by the first CME but the particle acceleration may be associated with shock–shock interaction. Therefore, 55% (6/11) of the events have the acceleration and SPR occurring much prior to the start of the CME–CME interaction. It is then interesting to study the effect of the different interacting types on the SEP Ip. Figure 7 shows the corresponding result. The  $x$ -axis denotes the

**Table 2**  
SEP Events in “Twin-CME” Scenario in Solar Cycle 24

SEP		CME									Type II
Onset	SPR	FAT <sub>C2</sub>	cpa	$v$	$w$	$(\phi, \theta)$	$v$	$\gamma$	$(w_f, w_e)$	Inter.	Onset
2011 Aug 9 08:20	08:05	pre 03:48	276°	1146	141°	(67°, 18°)	598	65°	(66°, 41°)	09:20	08:01
		pri 08:12	Halo	1610	360°	(59°, 9°)	1325	90°	(100°, 52°)		
2011 Nov 26 08:15	07:31	pre 00:36	250°	292	90°	(58°, -2°)	333	65°	(50°, 41°)	08:10	07:15
		pri 07:12	Halo	933	360°	(59°, 9°)	1029	90°	(179°, 50°)		
2012 Jan 23 04:45	04:22	pre 03:12	329°	684	221°	(23°, 23°)	874	-79°	(105°, 47°)	03:40	04:00
		pri 04:00	Halo	2175	360°	(16°, 41°)	1760	85°	(197°, 60°)		
2012 Mar 7 02:50	00:38	1st 00:24	Halo	2684	360°	(-37°, 18°)	2636	-90°	(121°, 58°)	01:25	00:17
		2nd 01:30	Halo	1825	360°	(-21°, 5°)	2397	-68°	(93°, 44°)		
2012 May 17 01:55	01:39	pre -	...	...	...	(63°, 0°)	1356	90°	(132°, 87°)	01:24	01:31
		pri 01:48	Halo	1582	360°	(94°, -11°)	1643	-69°	(64°, 29°)		
2012 Jul 8 18:10	17:02	pre 10:48	231°	662	61°	(73°, -47°)	602	-11°	(54°, 43°)	18:40	16:30
		pri 16:54	212°	1572	157°	(90°, -48°)	1086	12°	(113°, 61°)		
2013 May 15 06:35	01:56	pre 22:12 <sup>-1</sup>	46°	801	27°	(-95°, 50°)	888	0°	(47°, 47°)	04:00	01:37
		pri 01:48	Halo	1366	360°	(-70°, 10°)	1230	76°	(152°, 47°)		
2013 May 22 14:20	13:32	pre 08:48	270°	687	210°	(76°, 32°)	519	-73°	(92°, 47°)	13:41	12:59
		pri 13:25	Halo	1466	360°	(77°, 16°)	1439	-59°	(208°, 46°)		
2014 Jan 6 08:15	07:47	pre 00:36	276°	574	129°	(87°, 14°)	583	-90°	(75°, 43°)	09:25	07:45
		pri 08:00	Halo	1402	360°	(90°, 0°)	1347	-90°	(167°, 63°)		
2014 Apr 18 13:40	13:25	pre 07:24	209°	387	84°	(37°, -49°)	367	43°	(49°, 42°)	13:50	12:55
		pri 13:25	Halo	1203	360°	(40°, -32°)	1540	47°	(164°, 59°)		
2017 Sep 4 22:30	20:38	pre 19:00	233°	597	>205°	(25°, -7°)	913	90°	(67°, 45°)	20:45	20:27
		pri 20:36	Halo	1418	360°	(8°, -30°)	1785	14°	(119°, 47°)		

#### Notes.

[1] The table lists the information about the SEP onset time, SPR time, CME first appearance time in LASCO/C2 FOV, CME 2D parameters, CME 3D parameters, the start time of the CME-CME interaction and the onset time of the type II radio bursts. [2] The superscript of “-1” in the event on 2013 May 15 indicates that one day prior to the SEP onset day, i.e., on 2013 May 14. [3]  $v$  is the CME speed in the unit of km s<sup>-1</sup>, cpa and  $w$  are the central position angle and angular width of a CME in the CDAW/CME catalog. [4] The preCME in the event on 2012 May 17 cannot be identified in LASCO FOV.

normalized distance ( $d_n$ ) at the type II bursts onset time or the SPR time, which is derived as follows. First, if the priCME impacts the preCME, then  $d_n = 1 + \frac{h_{LE-priCME} - h_{TE-preCME}}{2R_{preCME}}$ , where  $h_{LE-priCME}$  is the height of the priCME LE, and  $h_{TE-preCME}$  and  $R_{preCME}$  are the height of the preCME TE and the radius of the preCME, respectively.  $d_n = 1$  refers to the time when the LE of the priCME rightly catches up with the TE of the preCME, and  $d_n = 2$  refers to the condition that the LEs of the two CMEs have fully merged. Note that  $d_n > 1$  does not imply that the magnetic ejecta of two CMEs are interacting or merging with each other, but it indicates that the priCME driven shock propagates inside the preCME. Second, if the priCME does not reach the preCME, then  $d_n = \frac{h_{LE-priCME}}{h_{TE-preCME}} < 1$ . The plots shows  $d_n$  versus SEP Ip, and each data point is shown by a diamond at SPR time accompanied with a horizontal bar whose left end refers to  $d_n$  at the onset time of the type II radio bursts. The speeds of the preCME and priCME are marked on the right and left of the data points. We take  $d_n = 2.1$  (considering a small sheath in front of the first CME) for the event on 2012 March 7 due to the potential shock-shock interaction. This figure shows that the SEP events will have relatively higher Ip if the particles are released at the time when the CMEs are meaningfully interacted or close to each other. In addition, based on Table 2, the estimated SPR time is about a

few to 30 minutes after the onset of the type II bursts, indicating the time needed for the particle acceleration by the shocks before they are released (also see Gopalswamy et al. 2012).

## 4. Discussion

### 4.1. Uncertainties in the Analyses

Hereafter we discuss the uncertainties in fitting the CME parameters, determining the interacting type, identifying the “twin-CME” events, and calculating the SPR time.

The typical uncertainties for the fitted parameters in the GCS models are given in Table 2 of Themisien et al. (2009) as: 4.3°, 1.8°, 0.48  $R_s$ , 0.07, 13°, and 22° for  $\phi$ ,  $\theta$ ,  $h$ ,  $\kappa$ ,  $\gamma$ , and  $\delta$ , respectively. The uncertainty of  $h$  is used in this paper. During the fitting, we fixed the CME parameters (except  $h$ ) as constants and used a linear fit to derive the speed, which ignores the deflection, lateral overexpansion, and speed variation of CMEs. CMEs are found to be deflected in the lower corona due to the asymmetric distribution of the background magnetic field (e.g., Gui et al. 2011; Shen et al. 2011; Möstl et al. 2015), and the lateral overexpansion refers to the fact that the radius (width) of the CME expands more strongly than it gains in height (see Veronig et al. 2018, and references therein). CMEs usually experience three stages of

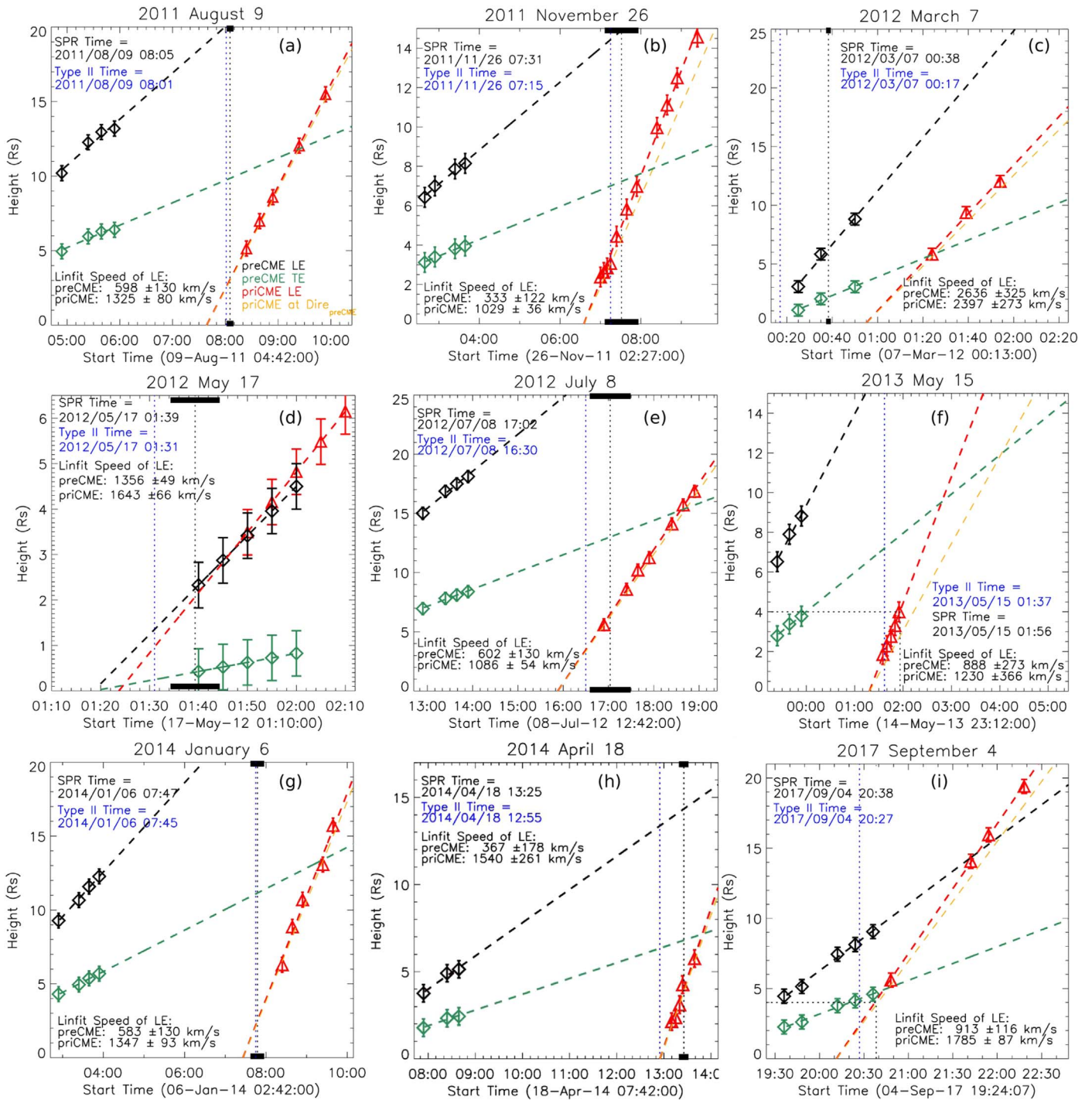


**Figure 6.** The interaction between the CMEs associated with the SPR and the type II radio bursts (similar to Figure 5).

dynamic evolution, i.e., a slow rise, a fast acceleration, and a propagation (Zhang et al. 2001, 2004). The fast acceleration occurs at very low coronal heights (e.g., Chen & Krall 2003; Temmer et al. 2008; Bein et al. 2011), and the propagation at higher heights is governed by the CME Lorentz force, the magnetic interaction with the corona and the drag force associated with interaction with the solar wind, leading to either slow acceleration or deceleration of CMEs (e.g., Michalek et al. 2015). These factors could influence the associated fitting parameters. Because we started the fits of the GCS model when the CME is at a relatively higher height, where the initial fast

acceleration has already ceased (see Section 3.1.1), the derived parameters could be seen as the average coronal values, which are reasonably used for our analyses.

The GCS model assumes the flux-rope structure of the CME instead of the shock, and the consideration of the shock driven by the priCME might affect the determination of the interacting type. The LE used in this paper is a good proxy for the shock position, and is what the GCS model is meant to track. The shock standoff distance ( $\Delta$ ) for the very fast priCMEs should be small in the low corona, because it is supposed to be inversely proportional to the square of the upstream Mach

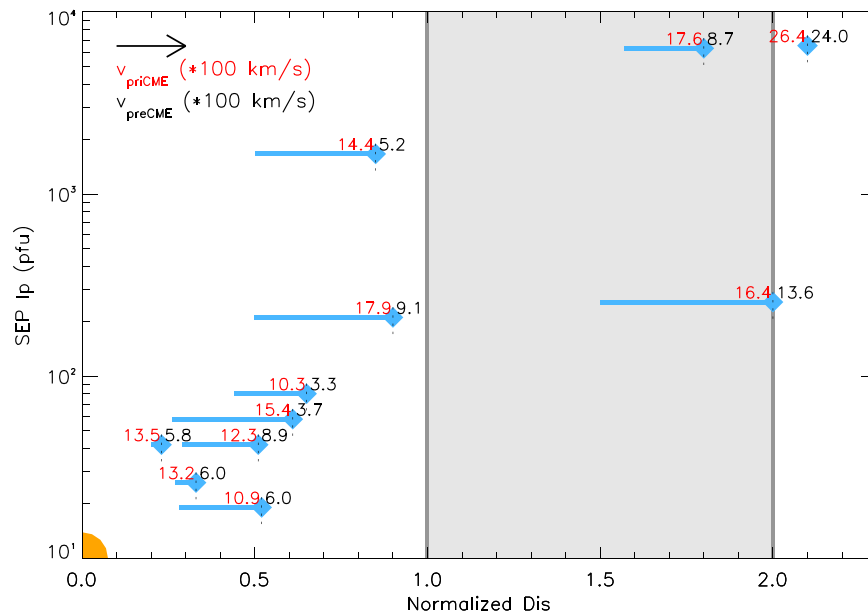


**Figure 7.** The acceleration and release of SEPs during the CME–CME interaction. Each data point is shown by a diamond at SPR accompanied with a horizontal bar whose left end refers to  $d_n$  at the onset time of the type II radio bursts. The numbers on the left and right of every data point refer to the 3D speed of the priCME and preCME, respectively. Two gray thick lines indicate the TE and the LE of the preCME, and the shadow area refers to the preCME area. The arrow indicates the outward propagation of a CME, and the orange quarter circle in the bottom left corner denotes the position of the Sun.

number (e.g., Savani et al. 2011, 2012). This is also confirmed by the observations of the events. Based on the previous studies (e.g., Gopalswamy & Yashiro 2011; Kim et al. 2012; Lee et al. 2017), we assume  $\Delta \sim 0.5 R_s$  at the height where the particles are accelerated for our “twin-CME” events. It is found that two events (on 2013 May 22 and 2017 September 4) for which the LE of the priCME is very close to the TE of the preCME, the shock propagation through the preCME could be possible. This will affect the related two data points, which are closest to the preCME TE in Figure 7, moving them rightward to the shadow area, but does not significantly change the six data points in the left part. Moreover, using a separate geometric model for the shock front (e.g., Mäkelä et al. 2015; Kozarev et al. 2015; Kwon & Vourlidas 2017; Kouloumvakos et al. 2019) could result in slightly more accurate timing of the shock–CME interaction but introduces a new assumption regarding the shock shape and a set of at least four new parameters. For simplicity’s sake, we consider that fitting the flux rope only may provide the most accurate picture for these fast CME events for which the standoff distance is small.

As described in Section 2.1, different criteria for identifying preCMEs would lead to different results. For example, the threshold of the speed might be different because the Alfvén speed in the low corona may vary in different coronal conditions and models (see, e.g., Gopalswamy et al. 2001a; Evans et al. 2008), and it will also affect  $\tau$  in return. The consideration of the angular width is also different because Ding et al. (2013) impose no threshold but Kahler & Vourlidas (2014) set the threshold as  $>10^\circ$ , and Gopalswamy et al. (2004) took the width  $>60^\circ$  but relaxed  $\tau < 24$  hr. We note that slight changes of the criteria, e.g., increasing  $\tau$  or decreasing the angular width of the preCME, do not significantly influence the 3D identification for our selected cases. In addition, it should be noted that the seed populations produced by the shock driven by a preCME could also contribute to enhanced acceleration of SEPs due to the potential cross-field diffusion (e.g., Zhang et al. 2009; Hu et al. 2017; Zhang & Zhao 2017;

Xie et al. 2019), even though the priCME does not overlap the preCME.

In the VDA, to accurately estimate the SPR time and path length, it is suggested by Wang & Qin (2015) that the SEP event should meet the following conditions: impulsive source duration, large parallel mean free paths, low background level, and good connectivity between the spacecraft and the source; the last one was re-emphasized by Ding et al. (2016). Note that the magnetic connectivity could also be modified by the eruption of the preCME(s) (Lugaz et al. 2009, 2010). Besides, the SPR time derived from the in-ecliptic measurements may be different from the real SPR time if the propagation direction of the CME is out of the ecliptic plane. The events on 2012 July 8, 2013 May 15, and 2017 September 4 show how these factors influence the VDA results. In addition, for the last two of the above three events, where the estimated path length did not look realistic, we also considered a height at SPR of  $4 R_s$  and determined the SPR time from this. This is a rough but effective assumption. Further studies shall be done by combining, for example, potential force-free source-surface model or magnetohydrodynamic (MHD) simulations for obtaining more realistic information in the corona.

#### 4.2. Factors Influencing the Acceleration of SEPs

In this paper, we are focusing on the association of the acceleration and release of SEPs with different types of CME–CME interaction. In fact, the particle acceleration process is a complex one involving many factors, e.g., (1) the CME (or shock) speeds (Richardson et al. 2015; Papaioannou et al. 2016; Kouloumvakos et al. 2019), (2) the shock parameters, e.g., Mach numbers, compression ratios, and shock geometry (Lee 1983; Kozarev et al. 2015; Kouloumvakos et al. 2019), (3) the magnetic connectivity between the spacecraft and the source (Richardson et al. 2014; Xie et al. 2019), (4) the level of seed particles, and (5) the level of turbulence (e.g., Wanner & Wibberenz 1993; Laitinen et al. 2018; Strauss & le Roux 2019).

Figure 2 shows a relationship between the CME 3D speed and the SEP Ip in NP<sub>3D</sub> group, which is consistent with the results in Kouloumvakos et al. (2019). The penultimate point has been widely discussed (e.g., Gopalswamy et al. 2004; Kahler & Vourlidas 2014; Ding et al. 2015), involving the role of the flare material and the interacting CMEs on seed particles. In Ding et al. (2015), the authors used a Fe/O ratio of 2.0 as the threshold for the presence of flare material and found that all events except one with Fe/O > 2.0 are in the “twin-CME” scenario, indicating the presence of flare seed material that are possibly from pre-flares. In Kahler & Vourlidas (2014), they proposed that higher SEP Ip could be explained by increases in both CME rates and seed particles during times of high solar activity instead of being due to CME–CME interaction. In Figure 7, the higher Ip in the cases of (nearly) interacting CMEs gives a hint that more seed particles will be accelerated if the priCME eruption is close to the preCME eruption, but it is still necessary to figure out which factor, i.e., the solar activity, the flare, or the preCME, mainly controls the level of the seed populations. The launch of the Parker Solar Probe (PSP) can contribute to this investigation in the future, because the spacecraft will reach as close as 8.86 R<sub>s</sub> from the solar surface by 2024. During its first two perihelion passages, a series of SEP events have been studied, focusing on the acceleration mechanisms and seed population preconditioning (see McComas et al. 2019; Schwadron et al. 2020).

## 5. Summary

The launch of the twin STEREO spacecraft enables the observations of CMEs from multiple viewpoints, and we now have a full solar cycle worth of measurements with multi-viewpoint observations (2007–2019). We study the large SEP events in SC24 by multi-viewpoint observations, and identify that for only 27% (11/41) of the events, the priCMEs can have spatial overlap with the preCMEs in 3D. This value is much smaller than the percentage (51%) derived by the identifications from single-viewpoint observation, and the previous statistical results in SC23 (e.g., Gopalswamy et al. 2004; Ding et al. 2013; Kahler & Vourlidas 2014). We find that the consideration of the 3D information results in fewer large SEP events being with potential twin CMEs than previously reported. We then analyzed the eleven events with successive CMEs with spatial overlap in 3D in detail, by combining the GCS model to study the propagation of the CMEs in 3D, using type II radio bursts to indicate the particle acceleration, and the VDA to estimate the release time of the SEPs. The role of the CME–CME interaction in the acceleration and release of the SEPs is the focus of our investigation. We find that, out of these 11 3D “twin-CME” events, there are six cases in which the priCME is far away from catching up with the back of the preCME when the SEPs are released. However, we also find that the SEP events have relatively higher Ip if the particles are released at the time when the CMEs are meaningfully interacted or close to each other. It makes the role of the CME–CME interaction somewhat unclear, but we propose that (i) the efficient acceleration and the following release of the SEPs do not require a meaningful interaction between CMEs, but (ii) such interaction, while rare, results in high Ip fluxes. The acceleration and release occur when the shock driven by the priCME reaches a certain height. The closer the primary shock is to the preCME (indicating the environment is more turbulent or with more seed populations), the higher SEP Ip

could be. In the future, we need more samples to confirm this finding, and the SEP events recorded by STEREO, or the recently launched PSP and Solar Orbiter could be helpful.

We thank the anonymous referee for the valuable suggestions. We acknowledge the use of the data from GOES, LASCO, and ERNE on board SOHO, STEREO/SECCHI, and WIND/WAVES. SOHO is a mission of international cooperation between ESA and NASA. The CME and SEP catalog used in this paper are generated and maintained at the CDAW Data Center by NASA and the Catholic University of America in cooperation with the Naval Research Laboratory. Research for this work was made possible by NASA grants 80NSSC17K0009 and 80NSSC19K0831, and NSF grant AGS1435785.

## ORCID iDs

Bin Zhuang  <https://orcid.org/0000-0002-5996-0693>  
 Noé Lugaz  <https://orcid.org/0000-0002-1890-6156>  
 Tingyu Gou  <https://orcid.org/0000-0003-0510-3175>  
 Liuguan Ding  <https://orcid.org/0000-0002-1799-5150>  
 Yuming Wang  <https://orcid.org/0000-0002-8887-3919>

## References

- Bein, B. M., Berkebile-Stoiser, S., Veronig, A. M., et al. 2011, *ApJ*, 738, 191  
 Brueckner, G. E., Howard, R. A., Koomen, M. J., et al. 1995, *SoPh*, 162, 357  
 Cane, H. V., Richardson, I. G., & von Roseninge, T. T. 2010, *JGRA*, 115, A08101  
 Chen, J., & Krall, J. 2003, *JGRA*, 108, 1410  
 Cliver, E. W. 2006, *ApJ*, 639, 1206  
 Colaninno, R. C., & Vourlidas, A. 2015, *ApJ*, 815, 70  
 Dayeh, M. A., Desai, M. I., Dwyer, J. R., et al. 2009, *ApJ*, 693, 1588  
 Démoulin, P., Klein, K. L., Goff, C. P., et al. 2007, *SoPh*, 240, 301  
 Ding, L., Jiang, Y., Zhao, L., & Li, G. 2013, *ApJ*, 763, 30  
 Ding, L.-G., Cao, X.-X., Wang, Z.-W., & Le, G.-M. 2016, *RAA*, 16, 122  
 Ding, L.-G., Li, G., Dong, L.-H., et al. 2014a, *JGRA*, 119, 1463  
 Ding, L.-G., Li, G., Jiang, Y., et al. 2014b, *ApJL*, 793, L35  
 Ding, L.-G., Li, G., Le, G.-M., Gu, B., & Cao, X.-X. 2015, *ApJ*, 812, 171  
 Ding, L.-G., Wang, Z.-W., Feng, L., Li, G., & Jiang, Y. 2019, *RAA*, 19, 005  
 Domingo, V., Fleck, B., & Poland, A. I. 1995, *SoPh*, 162, 1  
 Evans, R. M., Opher, M., Manchester, W. B., & Gombosi, T. I., I. 2008, *ApJ*, 687, 1355  
 Gopalswamy, N. 2012, in AIP Conf. Ser. 1436, Physics of the Heliosphere: A 10 Year Retrospective, ed. J. Heerikhuisen et al. (Melville, NY: AIP), 247  
 Gopalswamy, N., Aguilar-Rodriguez, E., Yashiro, S., et al. 2005, *JGRA*, 110, A12S07  
 Gopalswamy, N., Lara, A., Kaiser, M. L., & Bougeret, J. L. 2001a, *JGR*, 106, 25261  
 Gopalswamy, N., Mäkelä, P., Akiyama, S., et al. 2015, *ApJ*, 806, 8  
 Gopalswamy, N., Thompson, W. T., Davila, J. M., et al. 2009a, *SoPh*, 259, 227  
 Gopalswamy, N., Xie, H., Akiyama, S., et al. 2013, *ApJL*, 765, L30  
 Gopalswamy, N., Xie, H., Mäkelä, P., et al. 2010, *ApJ*, 710, 1111  
 Gopalswamy, N., Xie, H., Yashiro, S., et al. 2012, *SSRv*, 171, 23  
 Gopalswamy, N., & Yashiro, S. 2011, *ApJL*, 736, L17  
 Gopalswamy, N., Yashiro, S., Akiyama, S., et al. 2008, *AnGeo*, 26, 3033  
 Gopalswamy, N., Yashiro, S., Kaiser, M. L., Howard, R. A., & Bougeret, J. L. 2001b, *ApJL*, 548, L91  
 Gopalswamy, N., Yashiro, S., Krucker, S., Stenborg, G., & Howard, R. A. 2004, *JGRA*, 109, A12105  
 Gopalswamy, N., Yashiro, S., Lara, A., et al. 2003, *GeoRL*, 30, 8015  
 Gopalswamy, N., Yashiro, S., Michalek, G., et al. 2002, *ApJL*, 572, L103  
 Gopalswamy, N., Yashiro, S., Michalek, G., et al. 2009b, *EM&P*, 104, 295  
 Gui, B., Shen, C., Wang, Y., et al. 2011, *SoPh*, 271, 111  
 Guo, J., Dumbović, M., Wimmer-Schweingruber, R. F., et al. 2018, *SpWea*, 16, 1156  
 Howard, R. A., Moses, J. D., Vourlidas, A., et al. 2008, *SSRv*, 136, 67  
 Hu, J., Li, G., Ao, X., Zank, G. P., & Verkhoglyadova, O. 2017, *JGRA*, 122, 10938  
 Joshi, N. C., Uddin, W., Srivastava, A. K., et al. 2013, *AdSpR*, 52, 1

- Kahler, S. W. 1982, *ApJ*, 261, 710
- Kahler, S. W. 2001, *JGR*, 106, 20947
- Kahler, S. W., & Ling, A. G. 2019, *ApJ*, 872, 89
- Kahler, S. W., Ling, A. G., & Gopalswamy, N. 2019, *SoPh*, 294, 134
- Kahler, S. W., & Reames, D. V. 2003, *ApJ*, 584, 1063
- Kahler, S. W., Reames, D. V., & Burkepile, J. T. 2000, in ASP Conf. Ser. 206, A Role for Ambient Energetic Particle Intensities in Shock Acceleration of Solar Energetic Particles, ed. R. Ramaty & N. Mandzhavidze (San Francisco, CA: ASP), 468
- Kahler, S. W., & Vourlidas, A. 2005, *JGRA*, 110, A12S01
- Kahler, S. W., & Vourlidas, A. 2013, *ApJ*, 769, 143
- Kahler, S. W., & Vourlidas, A. 2014, *ApJ*, 784, 47
- Kaiser, M. L., Kucera, T. A., Davila, J. M., et al. 2008, *SSRv*, 136, 5
- Kim, R. S., Gopalswamy, N., Moon, Y. J., Cho, K. S., & Yashiro, S. 2012, *ApJ*, 746, 118
- Kouloumvakos, A., Patsourakos, S., Nindos, A., et al. 2016, *ApJ*, 821, 31
- Kouloumvakos, A., Rouillard, A. P., Wu, Y., et al. 2019, *ApJ*, 876, 80
- Kozarev, K. A., Dayeh, M. A., & Farahat, A. 2019, *ApJ*, 871, 65
- Kozarev, K. A., Evans, R. M., Schwadron, N. A., et al. 2013, *ApJ*, 778, 43
- Kozarev, K. A., Raymond, J. C., Lobzin, V. V., & Hammer, M. 2015, *ApJ*, 799, 167
- Kwon, R.-Y., & Vourlidas, A. 2017, *ApJ*, 836, 246
- Laitinen, T., Effenberger, F., Kopp, A., & Dalla, S. 2018, *JWSWC*, 8, A13
- Lee, J.-O., Moon, Y. J., Lee, J.-Y., Kim, R. S., & Cho, K. S. 2017, *ApJ*, 838, 70
- Lee, M. A. 1983, *RvGSP*, 21, 324
- Lemen, J. R., Title, A. M., Akin, D. J., et al. 2012, *SoPh*, 275, 17
- Li, G., Moore, R., Mewaldt, R. A., Zhao, L., & Labrador, A. W. 2012, *SSRv*, 171, 141
- Li, G., & Zank, G. P. 2005, Proc. ICRC (Pune), 1, 173
- Li, L. P., & Zhang, J. 2013, *A&A*, 552, L11
- Liu, Y. D., Luhmann, J. G., Kajdič, P., et al. 2014, *NatCo*, 5, 3481
- Lugaz, N., Farrugia, C. J., Davies, J. A., et al. 2012, *ApJ*, 759, 68
- Lugaz, N., Farrugia, C. J., Smith, C. W., & Paulson, K. 2015, *JGRA*, 120, 2409
- Lugaz, N., Manchester, W. B. I., & Gombosi, T. I. 2005, *ApJ*, 634, 651
- Lugaz, N., Roussev, I. I., & Sokolov, I. V. 2009, in IAU Symp. 257, Universal Heliophysical Processes, ed. N. Gopalswamy & D. F. Webb (Cambridge: Cambridge Univ. Press), 391
- Lugaz, N., Roussev, I. I., Sokolov, I. V., & Jacobs, C. 2010, in AIP Conf. Ser. 1216, Twelfth International Solar Wind Conference, ed. M. Maksimovic et al. (Melville, NY: AIP), 440
- Lugaz, N., Temmer, M., Wang, Y., & Farrugia, C. J. 2017, *SoPh*, 292, 64
- Mäkelä, P., Gopalswamy, N., Akiyama, S., Xie, H., & Yashiro, S. 2015, *ApJ*, 806, 13
- Mäkelä, P., Gopalswamy, N., Reiner, M. J., Akiyama, S., & Krupar, V. 2016, *ApJ*, 827, 141
- McComas, D. J., Christian, E. R., Cohen, C. M. S., et al. 2019, *Natur*, 576, 223
- Mewaldt, R. A., Mason, G. M., Cohen, C. M. S., et al. 2012, in AIP Conf. Ser. 1436, Physics of the Heliosphere: A 10 Year Retrospective, ed. J. Heerikhuisen et al. (Melville, NY: AIP), 206
- Michalek, G., Gopalswamy, N., Yashiro, S., & Bronarska, K. 2015, *SoPh*, 290, 903
- Miteva, R., Klein, K. L., Malandraki, O., & Dorrian, G. 2013, *SoPh*, 282, 579
- Möstl, C., Rollett, T., Frahm, R. A., et al. 2015, *NatCo*, 6, 7135
- Papaioannou, A., Sandberg, I., Anastasiadis, A., et al. 2016, *JWSWC*, 6, A42
- Pesnell, W. D., Thompson, B. J., & Chamberlin, P. C. 2012, *SoPh*, 275, 3
- Reames, D. V. 1995, *AdSpR*, 15, 41
- Reames, D. V. 1999, *SSRv*, 90, 413
- Reames, D. V. 2009a, *ApJ*, 706, 844
- Reames, D. V. 2009b, *ApJ*, 693, 812
- Reames, D. V. 2013, *SSRv*, 175, 53
- Richardson, I. G., von Rosenvinge, T. T., Cane, H. V., et al. 2014, *SoPh*, 289, 3059
- Richardson, I. G., von Rosenvinge, T. T., & Cane, H. V. 2015, *SoPh*, 290, 1741
- Savani, N. P., Owens, M. J., Rouillard, A. P., et al. 2011, *ApJ*, 732, 117
- Savani, N. P., Shiotani, D., Kusano, K., Vourlidas, A., & Lugaz, N. 2012, *ApJ*, 759, 103
- Schwadron, N. A., Bale, S., Bonnell, J., et al. 2020, *ApJS*, 246, 33
- Scolini, C., Chané, E., Temmer, M., et al. 2020, *ApJS*, 247, 21
- Shen, C., Li, G., Kong, X., et al. 2013a, *ApJ*, 763, 114
- Shen, C., Liao, C., Wang, Y., Ye, P., & Wang, S. 2013b, *SoPh*, 282, 543
- Shen, C., Wang, Y., Gui, B., Ye, P., & Wang, S. 2011, *SoPh*, 269, 389
- Shen, C., Wang, Y., Ye, P., & Wang, S. 2008, *SoPh*, 252, 409
- Shen, C., Xu, M., Wang, Y., Chi, Y., & Luo, B. 2018, *ApJ*, 861, 28
- Strauss, R. D., & le Roux, J. A. 2019, *ApJ*, 872, 125
- Temmer, M., Veronig, A. M., Peinhart, V., & Vršnak, B. 2014, *ApJ*, 785, 85
- Temmer, M., Veronig, A. M., Vršnak, B., et al. 2008, *ApJL*, 673, L95
- Thakur, N., Gopalswamy, N., Xie, H., et al. 2014, *ApJL*, 790, L13
- Thernisien, A. 2011, *ApJS*, 194, 33
- Thernisien, A., Vourlidas, A., & Howard, R. A. 2009, *SoPh*, 256, 111
- Thernisien, A. F. R., Howard, R. A., & Vourlidas, A. 2006, *ApJ*, 652, 763
- Török, T., Panasenco, O., Titov, V. S., et al. 2011, *ApJL*, 739, L63
- Torsti, J., Valtonen, E., Lumme, M., et al. 1995, *SoPh*, 162, 505
- Tylka, A. J., Cohen, C. M. S., Dietrich, W. F., et al. 2003, Proc. ICRC (Tsukuba), 6, 3305
- Vainio, R., Valtonen, E., Heber, B., et al. 2013, *JWSWC*, 3, A12
- Veronig, A. M., Podladchikova, T., Dissauer, K., et al. 2018, *ApJ*, 868, 107
- Wang, X., Giacalone, J., Yan, Y., et al. 2019, *ApJ*, 885, 66
- Wang, Y., & Qin, G. 2015, *ApJ*, 806, 252
- Wanner, W., & Wibberenz, G. 1993, *JGR*, 98, 3513
- Xie, H., St., Cyr, O. C., Mäkelä, P., & Gopalswamy, N. 2019, *JGRA*, 124, 6384
- Xu, M., Shen, C., Chi, Y., et al. 2019, *ApJ*, 885, 54
- Yashiro, S., Gopalswamy, N., Mäkelä, P., et al. 2014, *AdSpR*, 54, 1941
- Yashiro, S., Gopalswamy, N., Michalek, G., et al. 2004, *JGRA*, 109, A07105
- Zhang, J., Dere, K. P., Howard, R. A., Kundu, M. R., & White, S. M. 2001, *ApJ*, 559, 452
- Zhang, J., Dere, K. P., Howard, R. A., & Vourlidas, A. 2004, *ApJ*, 604, 420
- Zhang, M., Qin, G., & Rassoul, H. 2009, *ApJ*, 692, 109
- Zhang, M., & Zhao, L. 2017, *ApJ*, 846, 107